

Correlating welding reaction stresses and weld process conditions for high-strength steel S960QL

Dirk Schropfer · Thomas Kannengiesser

Received: 25 October 2013 / Accepted: 10 March 2014 / Published online: 28 March 2014
© International Institute of Welding 2014

Abstract As a result of current trends towards lightweight design, a growing amount of high-strength steels with yield strengths above 690 MPa is applied. In comparison to the weld process of lower-strength steels, small working ranges have to be achieved with respect to a special microstructure and high yield ratio. However, the sustainable and economic application of these steels depends on the loading capacity and the safety of welds when designing weld constructions. For these demands, a precise knowledge of welding stress level and distribution is essential. Therefore, the present study is concerned with the interaction between heat control (interpass temperature and heat input) and local as well as global stresses in high-strength steel welds. Specimens were multirun welded under defined restraint conditions in a special test facility (controlled tensile weldability (CTW) test) to consider global restraint. For the comparison concerning local residual stresses, free shrinkage test welds were performed as well. The evaluation shows a significant influence of the interpass temperature on the global reaction forces. Furthermore, increased heat input and high interpass temperatures cause higher tensile residual stresses. This occurred in the weld area of both free shrinkage test specimen and CTW test specimen.

Keywords Residual stresses · MAG welding · Restraint · High-strength steels · Process parameters

Doc. IIW-2442, recommended for publication by Commission II “Arc Welding and Filler Metals”

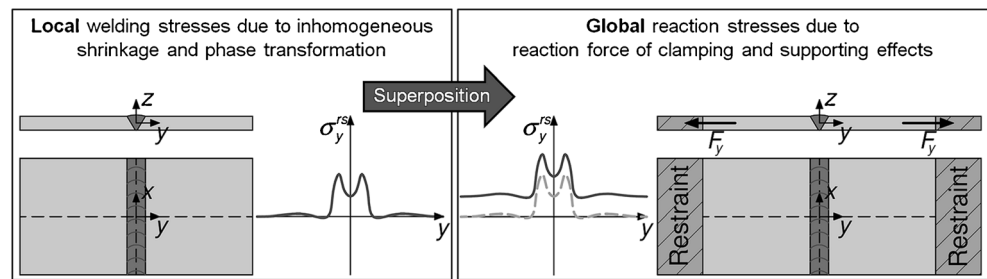
D. Schropfer (✉) · T. Kannengiesser
BAM Federal Institute for Materials Research and Testing, Berlin,
Germany
e-mail: dirk.schropfer@bam.de

T. Kannengiesser
e-mail: thomas.kannengiesser@bam.de

1 Introduction

In an increasing number of industries, high-strength fine-grained structural steels are applied in modern steel constructions [1, 2]. Today’s steel market provides a wide range of weldable high-strength base materials. High savings in weight and production costs are possible, depending on the material strength [3, 4]. For an economical application of these steels, the exhaustion of load capacity and simultaneous consideration of advanced safety requirements are necessary. Hence, the major objectives of the weld heat control are the compliance of the required microstructure and properties as well as sufficient hydrogen effusion and the avoidance of any crack initiations. Therefore, the cooling time from 800 °C to 500 °C ($\Delta t_{8/5}$ cooling time) is broadly accepted as a practical indicator [5]. In order to estimate the weld thermal cycle, many empirical approaches, e.g. based on the carbon equivalent and testing methods, were developed [6]. In addition to the metallurgical aspects, a reduction of residual stresses improves crack prevention as well. This reduction can be accomplished by an appropriate heat control before, during and after welding [7]. Therefore, a detailed forecast of welding stresses is necessary, especially when welding high-strength steels. So far, most research activities are concerned with residual stress characteristics in welds of free-shrinking laboratory samples [8]. However, estimating welding stresses requires a sufficient knowledge about the interaction between heat control, material and restraint of surrounding structures [7, 9, 10]. Avoiding crack critical reaction stresses and providing adequate mechanical properties depend on adequate heat control parameters. The influence of restraint conditions on the stress development was analysed in several numerical and experimental works. These studies revealed a high effect of restraint intensity and component dimensions on reaction stresses in welded structures [11, 12]. Therein, local residual stresses are superimposed by global reaction stresses due to the additional

Fig. 1 Welding stresses as a result of local and global restraint [11]



external shrinkage restraint, cp. Fig. 1. Depending on the stiffness of weld constructions, the magnitude of maximum residual stresses in the weld seam area can attain a crack critical level [11, 13]. For that purpose, analyses considering the interaction between heat control and stress build-up level were realised by [14].

In most cases, expected welding stresses are considered via global safety factors in the prevailing standard and technical guidelines, e.g. EN 1011-2 [6] and EC 3 [15]. Continuitive studies for further improvements of this issue are missing so far. Hence, this present study is concerned with the influence of the weld thermal cycle on the stresses in high-strength steel welds considering effects due to an external restraint.

2 Experimental

As test material, plates of high-strength quenched and tempered fine-grained structural steel EN 10025-6 S960QL [16] with a thickness of 8 mm were used. The filler material was the similar high-strength solid wire according to ISO 16834-A-G 89 6 M Mn4Ni2CrMo [17]. The chemical composition and mechanical properties are given in Tables 1 and 2. All welds were accomplished with an automated MAG multilayer welding process. The welding parameters are shown in Table 3.

Initially, free shrinkage weld tests were made. Thus, the influence of heat control parameters on cooling rates and local residual stresses was investigated. Moreover, these specimens were tested according to ISO 15614-1 [18] to ensure the required mechanical properties of the weld. To realise an

implementation of a defined restraint in transverse direction during welding and cooling, the specimens were clamped into the controlled tensile weldability (CTW) test facility (Figs. 2 and 3). For comparison reasons, considering resulting global restraints in different weld constructions, the restraint intensity R_{F_y} was established. The restraint intensity in weld transverse direction R_{F_y} is the component stiffness towards the weld seam based on the seam length. It can be estimated for simple butt joints according to [19]. The restraint intensity was kept constant $R_{F_y}=2$ kN/(mm·mm) in all CTW tests.

Additionally, run-on/off plates were attached to the specimens to minimise influences of instable arc conditions during ignition and shut-off. The variation of heat control was realised by a modification of the interpass temperature T_i and heat input E using design of experiments (cp. Table 4). The heat input was modified via welding speed to achieve a preferably constant heat output if possible. Though, weld current and voltage were merely adjusted to accomplish a stable welding process (cp. Table 3). Regarding production-relevant process conditions, the $\Delta t_{8/5}$ cooling times had to be considered while selecting heat control parameters.

During all weld tests, preheat and interpass temperatures were observed using type K thermocouples attached 10 mm adjacent to the weld seam. In addition, the interpass temperature was monitored with a contact thermocouple on the weld. The determination of the $\Delta t_{8/5}$ cooling times was realised by an optical temperature measurement at the weld layer surface using a two-colour pyrometer (measuring range 350 to 1,300 °C). Furthermore, in the CTW tests, the reaction force was measured in real time while welding and cooling to ambient temperature. The local residual stresses in the weld

Table 1 Chemical compositions of test materials (spark emission spectroscopy)

Element (%) ^a	C	Si	Mn	B	Cr	Cu	Mo	Nb	V	Ni	Ti	CET ^d
Base material ^b	0.12	0.23	1.27	0.0007	0.20	0.01	0.59	0.015	0.050	0.059	0.01	0.32
Filler material ^c	0.11	0.71	1.47	0.0010	0.35	0.11	0.62	0.001	0.002	2.21	0.03	0.40

^a Residual Fe

^b EN 10025-6 S960QL [16]

^c EN ISO 16834-A-G 89 6 M Mn4Ni2CrMo [17]

^d EN 1011-2 [6]

Table 2 Mechanical properties of the test materials

Property	Yield strength $R_{p0,2}$ (MPa)	Tensile strength R_m (MPa)	Elongation at fracture A_5 (%)	Contraction at fracture Z (%)	Impact toughness A_v at -40 °C (J)	Hardness (HV10)
Base material ^a	960	980 bis 1,150	Min. 12	–	Min. 27	336 ^c
Filler material ^b	954	1,024	14.6	40.7	52	345

^a EN 10025-6 S960QL [16], properties under standard

^b EN ISO 16834-A-G 89 6 M Mn4Ni2CrMo [17], properties from producer test report

^c Hardness testing

seam area were measured via X-ray diffraction using the $\sin^2\psi$ method on the top surface after cooling to ambient temperature. Specimens from CTW tests were declamped before residual stress measurements, because of accessibility reasons.

$$\Delta t_{8/5} = 0.31 + 6.86E - 0.097T_i + 0.22E \cdot T_i$$

($\Delta t_{8/5}$ in s, E in kJ/mm, T_i in °C).

3 Results

3.1 $\Delta t_{8/5}$ cooling times

Figure 4a presents a statistical evaluation of the determined $\Delta t_{8/5}$ cooling times within the analysed working range. By use of design of experiments, an efficient evaluation of the effects and interaction of the factors is possible. Within these statistical analyses, the p value is a coefficient used to quantify the effect significance of each factor. If $p > 0.05$, the particular factor has a significant effect since it exceeds the level of significance of 5 %. It is obvious that the $\Delta t_{8/5}$ cooling times are significantly affected by both parameters interpass temperature T_i and heat input E . Also, an interaction of both parameters $T_i \cdot E$ was observed. Hence, the effect of the interpass temperature on the $\Delta t_{8/5}$ cooling time increases with higher values of the heat input (cp. Fig. 4b). However, these determined $\Delta t_{8/5}$ cooling times are divergent compared to the results of empirical relations for $\Delta t_{8/5}$ cooling time forecast, used in the prevailing technical guidelines and standards (e.g. EN 1011-2 [6]). The measured $\Delta t_{8/5}$ cooling time is on average 2 s longer, apparently due to different specimen dimensions and conditions of heat conduction in the present case of weld test specimen. Moreover, from the applicatory point of view, it can be said that the $\Delta t_{8/5}$ cooling time is affected by the heat input rather than by the interpass temperature. Within this working range, the following functional relation persists:

3.2 Reaction forces and stresses

In Fig. 5, the reaction force $F_y(t)$ and temperature $T(t)$ are shown for the CTW test R4. Starting at the root, the reaction force is $F_y = -2.4$ kN, since the preheating of the tack-welded specimen causes a low initially compressive force. A considerable force build-up can be observed during the root-run weld because the already inserted solidified weld metal generates transversal shrinking forces. The reaction force increases further as the temperature is decreasing during cooling to interpass temperature. At $T_i = 50$ °C, a first maximum of $F_y = 59$ kN due to restrained shrinkage occurs. During welding of the next run, the reaction force decreases because a local heat input combined with stress relief and a partial fusion of the root weld occurs. Subsequent cooling to T_i leads to a new continuous increase of the reaction force. During welding and subsequent cooling of the top layer, a similar development appears. But a maximum reaction force of $F_{y, \text{end}} = 90$ kN was measured at ambient temperature. Moreover, the amplitude of the transient reaction force reduction is a result of the welding heat input. This amplitude increases with each layer. Also, the rise of the reaction force during subsequent cooling to interpass temperature grows with every weld sequence.

Figure 6a shows reaction forces $F_y(t)$ for CTW tests with interpass temperatures of $T_i = 50$ °C and $T_i = 110$ °C. The two $F_y(t)$ graphs exhibit the same tendency. Obviously, the increased interpass temperature of $T_i = 110$ °C leads to a reduction of total welding time Δt_w by 71 %. A comparison of the amplitudes of reaction forces at the particular weld sequence

Table 3 Welding parameters

Weld preparation	Welding current, voltage	Welding speed	Wire feed speed	Shielding gas
V groove; 45°	240 A ± 20 A, 23 V ± 1.5 V	390 mm/min to 550 mm/min	6 m/min to 7 m/min	ISO 14175-M21-ArC-18 [22]

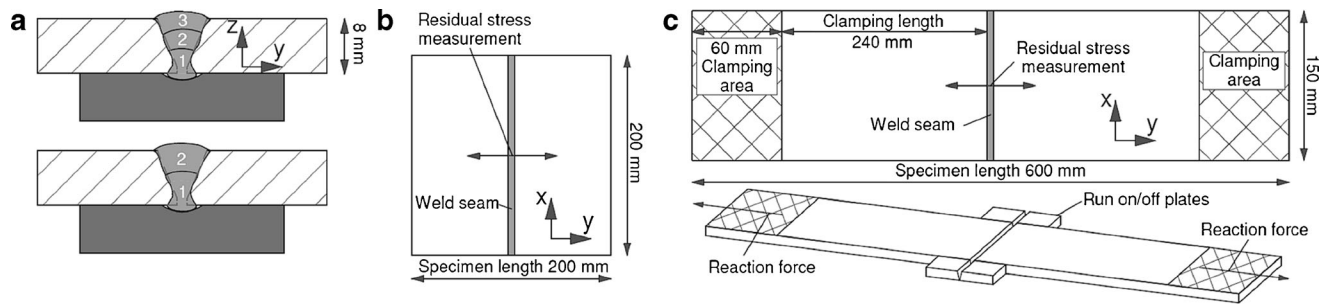


Fig. 2 Specimen dimensions. **a** Weld run sequence, **b** free shrinkage weld, **c** CTW test specimen

reveals further quantitative deviations of the $F_y(t)$ graphs. These force amplitudes are much smaller while welding with increased interpass temperature, since shorter cooling phases are involved. This causes a higher remaining heat between the weld runs. Hence, the reduction of transverse shrinking forces is comparatively low at the particular weld sequence. Remarkably, at the beginning of subsequent cooling of the top layer to ambient temperature, the reaction force is about $\Delta F_y = 15$ kN lower while welding with higher interpass temperature. But, it is assumed that this specimen contains a higher total heat quantity after the top layer weld run due to shorter cooling phases. Hence, an increased reaction force and, accordingly, reaction stress after cooling to ambient temperature results. In this case, at comparatively low restraint intensity, the increase approximates 20 %.

Furthermore, Fig. 6b shows the influence of the heat input E on the reaction force $F_y(t)$ with a constant interpass temperature T_i . Although only two instead of three runs were required to fill up the weld seam, the end reaction force is slightly higher when welding with increased heat input. Apparently, an increased heat input leads to a steeper rising of the reaction force during cooling to interpass temperature. Additionally, a higher total heat quantity after the top lay weld run is presumed, which induces higher transverse shrinking forces similar to the case of increased interpass temperature. In Fig. 7a the statistical evaluation for the reaction stresses in weld transverse direction after cooling to ambient temperature $\sigma_{y, \text{end}}$ is presented by a contour plot. These reaction stresses were calculated by means of the measured reaction forces based on the specimen cross section

($A = 150 \text{ mm} \cdot 8 \text{ mm}$). The results are in accordance with earlier research studies [11, 14, 23]. The end reaction stress is significantly influenced by the interpass temperature in the chosen working range. Finally, Fig. 7b reveals that the highest influence of the interpass temperature on the end reactions stress $\sigma_{y, \text{end}}$ occurs at low heat input values respectively where more weld-runs are required.

3.3 Local residual stresses in the weld seam area

Primarily, the analyses were focused on relations between local transverse residual stresses σ_y^{rs} and heat control, since global restraint conditions are applied in transverse direction as well. In particular, high effects are presumed due to restraint intensity. Figure 8 presents the transversal residual stress distributions across the weld for two different interpass temperatures at the centre line ($x=0$ mm) of the specimen welded under free shrinkage (a) and the declamped CTW test specimen (b). Both graphs show typical transversal residual stress distributions for steels including phase transformation effects according to common concepts [20, 21]. The tensile stress rises to a maximum of about 700 MPa (70 % of $R_{p0.2}$ of the weld metal), if the high interpass temperature was used. Since increased interpass temperature involves shorter cooling phases, the remaining heat quantity in the weld is higher while the top layer is welded (cp. Section 3.2 and Fig. 6a). In that case, the subsequent cooling to ambient temperature causes an increased inhomogeneous shrinkage restraint in the weld area.

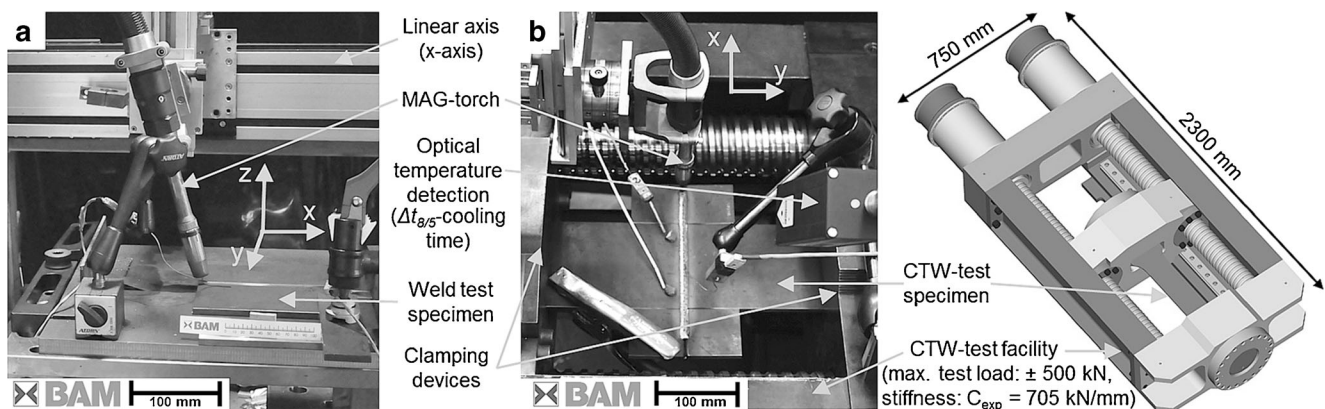


Fig. 3 Test setup. **a** Free shrinkage weld test, **b** CTW test and schematic pattern of the test facility

Table 4 Design of experiments and process conditions for the variation of heat control

Test no.	1	2	3	4	5	6	7	8
Preheat temperature T_p (°C)	50	50	50	50	50	50	50	50
Interpass temperature T_i (°C)	110	80	50	50	110	130	80	80
Heat input E (kJ/mm)	0.6	0.7	0.8	0.6	0.8	0.7	0.53	0.87
Free shrinkage	F1	F2	F3	F4	F5	F6	F7	F8
CTW test	R1	R2	R3	R4	R5	–	–	–

Fig. 4 Statistical evaluation of $\Delta t_{8/5}$ cooling times (model quality $R^2=94.8\%$, E is significant ($p<0.001$), T_i is significant ($p<0.001$), $T_i \cdot E$ is significant ($p=0.031$), level of significance 5%). **a** $\Delta t_{8/5}$ cooling times versus interpass temperature T_i and heat input E , **b** mean $\Delta t_{8/5}$ cooling times versus interpass temperature T_i for two values of heat input E

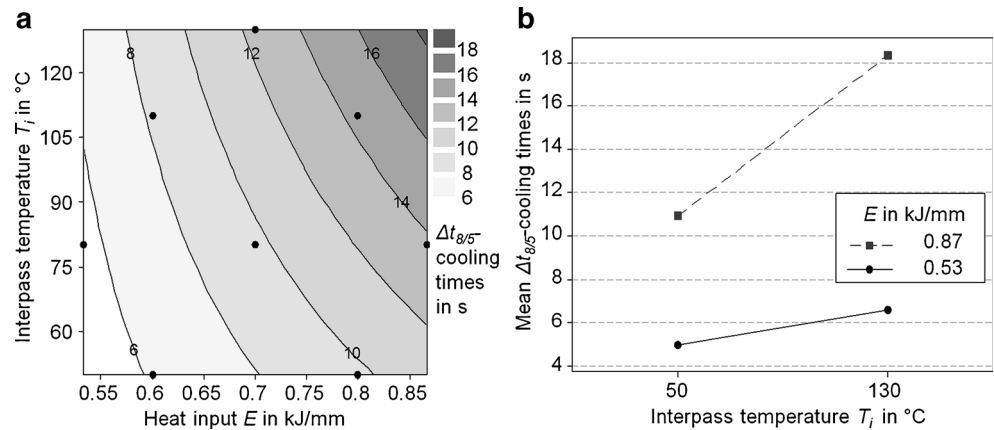
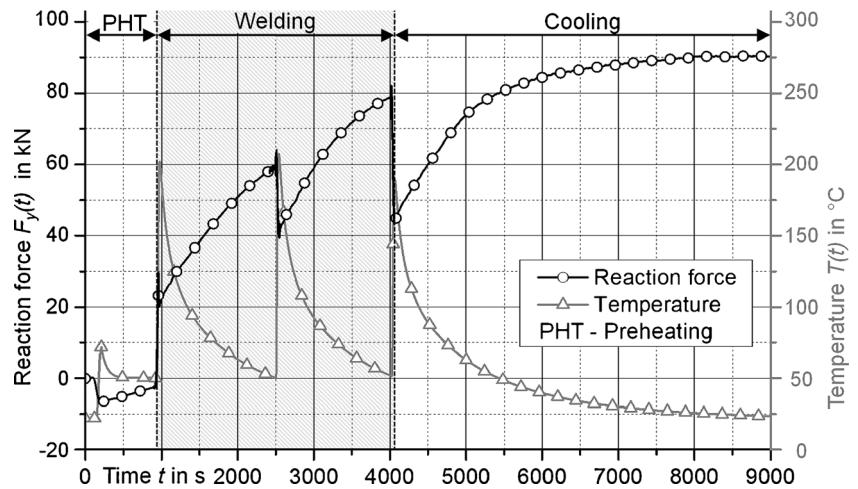


Fig. 5 Reaction force $F_y(t)$ and temperature $T(t)$ (number of runs 3, $T_p=50$ °C, $T_i=50$ °C, $E=0.6$ kJ/mm, $\Delta t_{8/5}=6.4$ s)



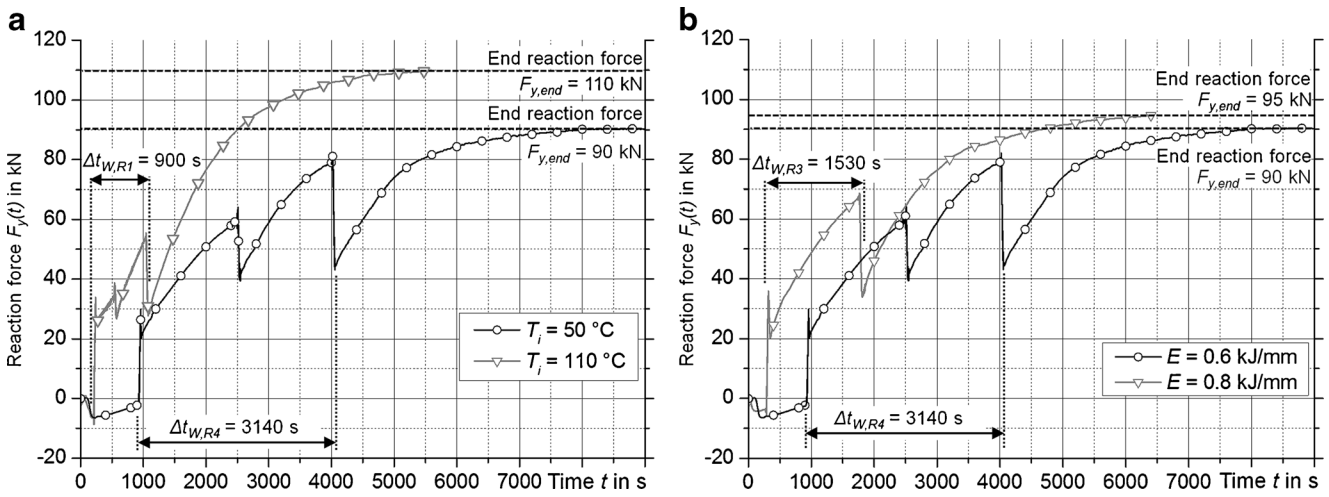


Fig. 6 Comparison of reaction force graphs $F_y(t)$. **a** $F_y(t)$ for two different interpass temperatures, $E=0.6$ kJ/mm. **b** $F_y(t)$ for two different values of heat input, $T_i=50$ °C

Hence, the initiation of tensile stresses is corresponding. Furthermore, cooling times above $\Delta t_{8/5}=10$ s lead to increased M_s and M_f temperatures. Around $\Delta t_{8/5}=15$ s, the transformation temperatures are about 50 °C higher. Apparently, the content of bainitic phase in the predominantly martensitic microstructure of the weld metal grows above $\Delta t_{8/5}=10$ s and causes an additional increase of the residual stresses according to previous studies [21].

A higher heat input similarly affects increased transversal tensile stresses in the weld area (cp. Fig. 9). Furthermore, the higher heat input causes an expansion of the stress distribution profile. Though, this could be primarily observed at free shrinkage test specimen (a). The reason is a larger volume of heated material and, hence, an augmentation of the involved inhomogeneous shrinking process. The measurements of the free shrinkage specimen are qualitatively consistent with the deplumped CTW test

specimen measurements. Also, the quantitative deviation is less than the measurement error. Since the superposition of global and local stresses at the CTW test specimen was not measured due to accessibility reasons, the effect of the restraint intensity could not be identified at this point.

Furthermore, Fig. 10a reveals the effect of the heat cycle by a statistical evaluation of the average transversal tensile residual stresses over the weld seam area ($y=-6$ to $+6$, $x=0$) $\sigma_{y, avg}^{rs}(-6... +6)$ using a contour plot. The maximum influence of the heat input occurred within increased interpass temperatures, and the influence of the interpass temperature rises with increasing heat input. Both parameters have a significant effect similar to the $\Delta t_{8/5}$ cooling time (cp. Fig. 4). The relationship of the maximum transversal tensile residual stress $\sigma_{y, max}^{rs}$ to the $\Delta t_{8/5}$ cooling time shown in Fig. 10b reveals a linear

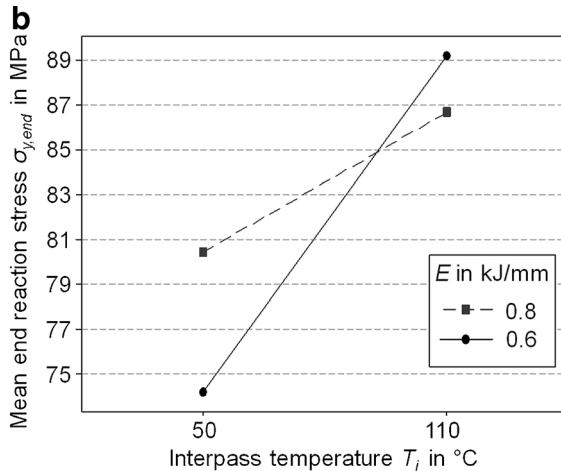
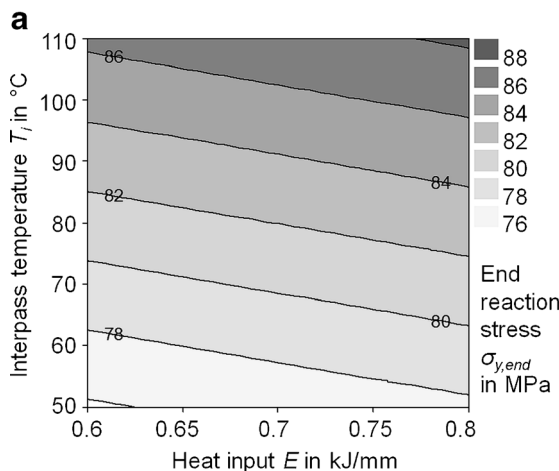


Fig. 7 Statistical evaluation of reaction stresses in weld transversal direction due to restraint in the CTW test facility after cooling to ambient temperature $\sigma_{y, end}$ (model quality $R^2=69.67$ %, E is not significant ($p=0.45$), T_i is significant ($p=0.002$), $T_i \cdot E$ is not significant, level of signif-

icance 5 %). **a** Reaction stresses $\sigma_{y, end}^{rs}$ versus interpass temperature T_i and heat input E . **b** Reaction stresses $\sigma_{y, end}^{rs}$ versus interpass temperature T_i for two values of heat input E

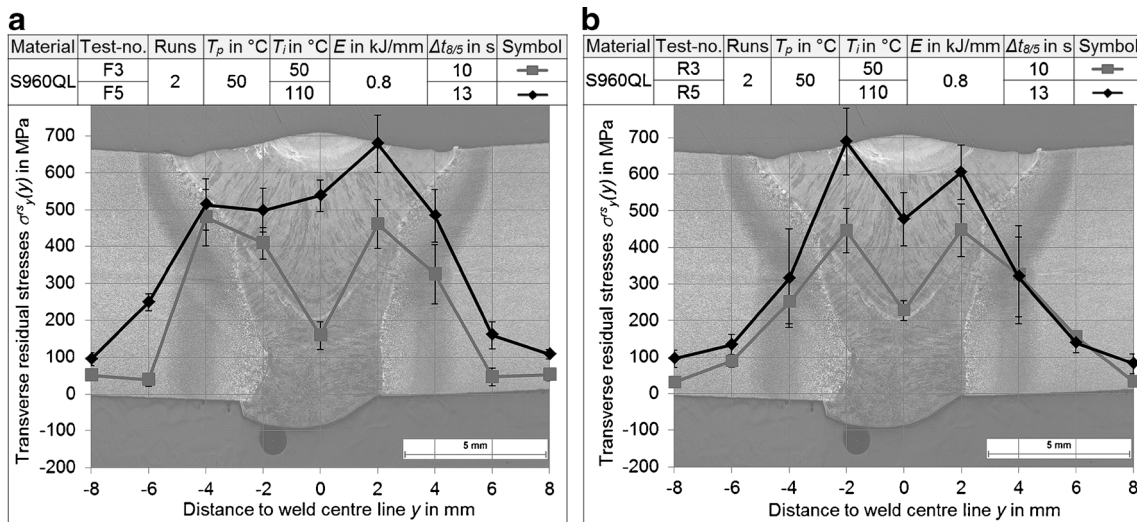


Fig. 8 Transverse residual stresses $\sigma_y^{rs}(y)$ on the weld seam at $x=0$ mm (seam centre) for two different interpass temperatures T_i , $E=0.8$ kJ/mm. **a** Free shrinkage test specimen. **b** CTW test specimen, declamped

correlation. However, a wide scatter is evident at the maximum transverse tensile residual stresses. Apparently, the residual stress distributions (cp. Figs. 8 and 9) exhibit these deviations among the two maximum tensile stresses in the weld seam as well as the measurement uncertainties in the weld metal area.

3.4 Superposition of global and local stresses

In case of low restraint intensities, an elastic approach considering superposition of local and global stresses can be provided. Hence, it is assumed that the local transverse residual

stresses decrease by the amount of the global end reaction stress while declamping the specimen welded under restraint condition. In reverse, the local transverse residual stresses measured at the declamped CTW test specimen can be superimposed with the measured end reaction stress $\sigma_{y, end}$ [12]. This causes an offset in tensile direction, as long as there is no plastic deformation. The resulting residual stresses should not rise above the yield strength of the material. Figure 11 shows the residual stress distribution in weld transverse direction for a CTW test specimen welded with $E=0.7$ kJ/mm and $T_i=80$ °C and the assumed residual stress distribution with an offset of end reaction stress of $\sigma_{y, end}=82$ MPa.

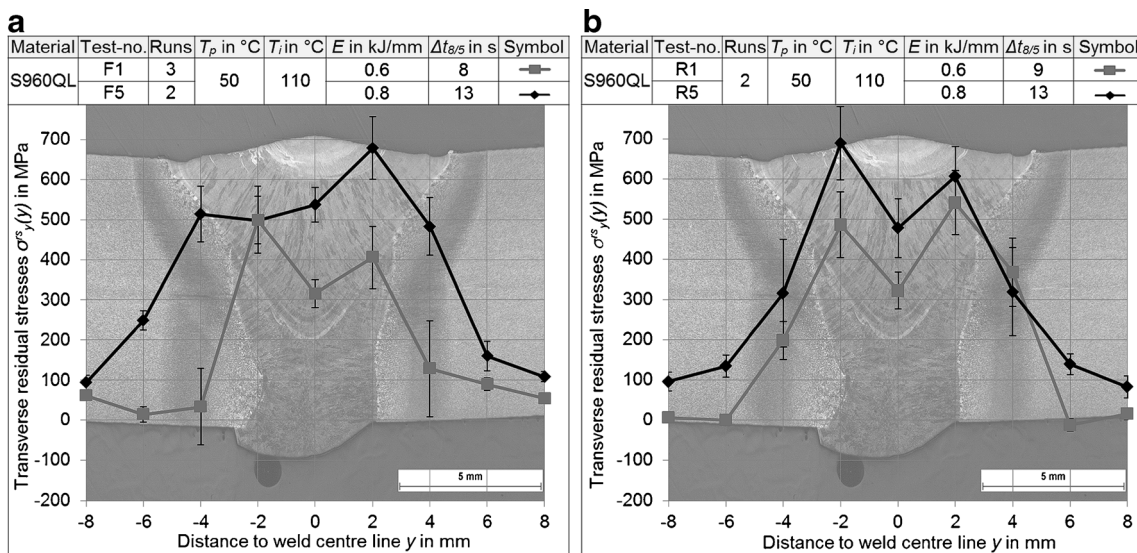


Fig. 9 Transverse residual stresses $\sigma_y^{rs}(y)$ on the weld seam at $x=0$ mm (seam centre) for two different values of heat input E , $T_i=110$ °C. **a** Free shrinkage test specimen. **b** CTW test specimen, declamped

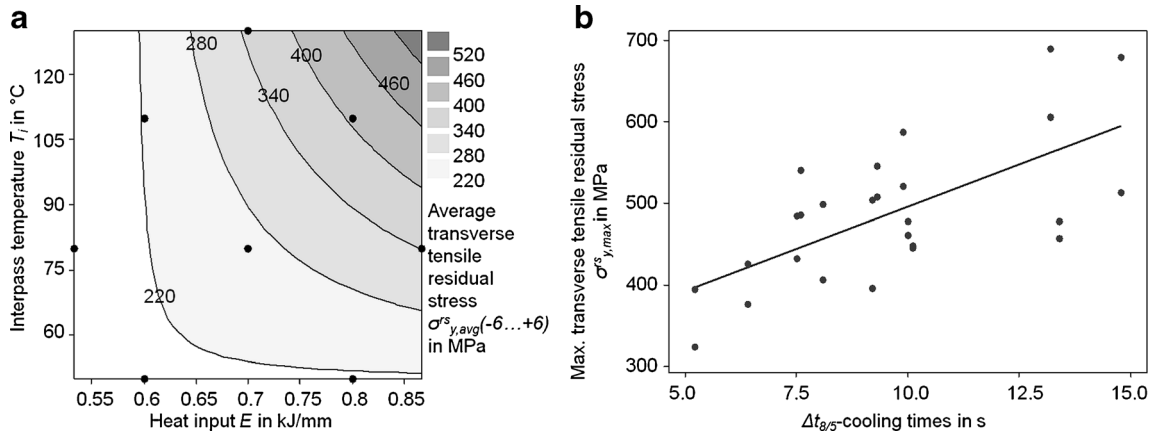


Fig. 10 Statistical evaluation of transverse tensile residual stresses $\sigma_y^{rs}(-y)$ at weld seam area of free shrinkage test specimen ($x=0$ mm, seam centre). **a** Average stress $\sigma_y^{rs}, \text{avg}(-6...+6)$ versus T_i and E (model quality)

$R^2=80.2\%$, E is significant ($p<0.001$), T_i is significant ($p=0.001$), $T_i \cdot E$ is significant ($p=0.011$), level of significance 5%. **b** Maximum stress $\sigma_y^{rs}, \text{max}$ versus $\Delta t_{8/5}$ cooling time, linear regression

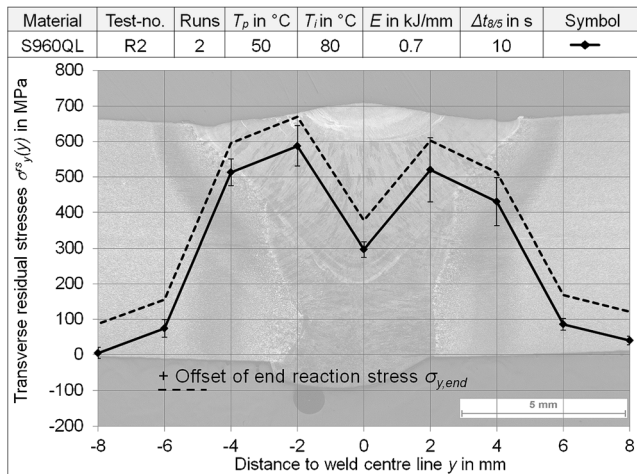


Fig. 11 Transversal residual stress distribution $\sigma_y^{rs}(y)$ at the weld seam area of declamped CTW test specimen ($x=0$ mm, seam centre) for $E=0.7$ kJ/mm and $T_i=80$ °C, plus offset of the end reaction stress $\sigma_{y, \text{end}}$ due to superposition (dashed line)

Finally, the statistically evaluated data of the average transverse tensile residual stresses $\sigma_y^{rs}, \text{avg}$ of the weld area versus the interpass temperature for two different heat input values are compared in Fig. 12. Figure 12a shows the local stresses in the specimen welded under free shrinkage condition. In Fig. 12b, the local stresses are superimposed by the end reaction stress offset, measured after the cooling of the CTW test specimen to ambient temperature. It reveals a significant influence of the heat input on local stresses in both test series, especially for high interpass temperatures. Under restraint, however, the influence of the interpass temperature on the local stresses is considerably higher at low heat input. Though, comparatively low restraint intensities were present while welding [10]. Further examinations should be made on appropriate specimen and test facility dimensions as well as higher restraint intensities.

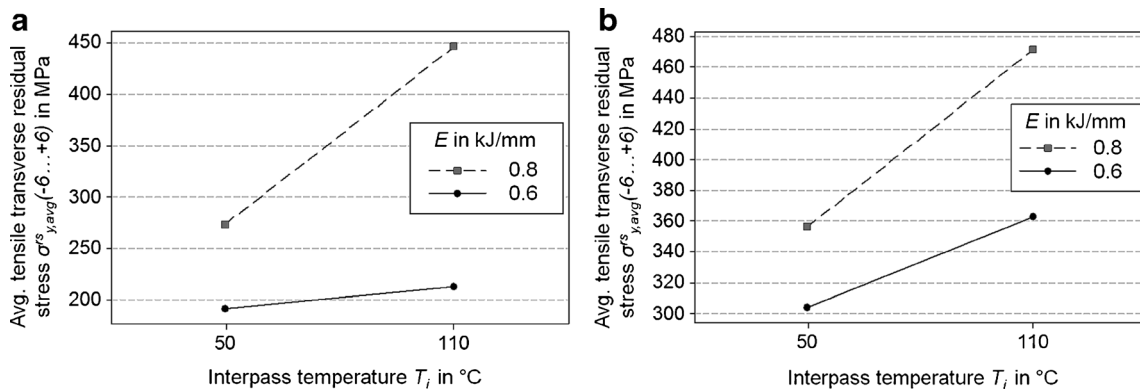


Fig. 12 Mean values of the average transverse tensile residual stress $\sigma_y^{rs}, \text{avg}(-6...+6)$ versus interpass temperature T_i for two values of heat input E in the weld seam area for free shrinkage and declamped CTW test

specimens plus an offset of the particular end reaction stresses. **a** Specimen welded under free shrinkage conditions. **b** Declamped CTW test specimen plus an offset of the particular end reaction stress $\sigma_{y, \text{end}}$

4 Conclusions

In the present study, the influence of heat control on local and global welding stresses in high-strength steel welds was analysed by means of interpass temperature and heat input variation. Free-shrinking multilayer welds were realised in order to focus on cooling rates, mechanical properties and local residual stresses. For the consideration of the global restraint in welded structures, specimens were welded under defined restraint intensity in weld transverse direction. The following conclusions can be drawn:

1. The $\Delta t_{8/5}$ cooling time is strongly influenced by the heat control. Since the cooling rate primarily determines the intended microstructure properties [5], it exhibits the attainment of adequate strength and toughness. From the applicatory point of view, the $\Delta t_{8/5}$ cooling time is mostly affected by the heat input in these analyses. However, it cannot be used as an indicator for the level of reaction forces and stresses.
2. The local residual stresses in the weld seam area are influenced by the heat control. Furthermore, for the free shrinkage test specimen, it was found that the magnitude of the occurring transverse tensile residual stresses correlates with the $\Delta t_{8/5}$ cooling time.
3. The heat control directly influences the reaction stress in weld transverse direction. A major dependence was observed within the interpass temperature despite the comparatively low restraint intensity. High interpass temperatures lead to increased reaction stresses.
4. The determined local stresses of the declamped CTW test specimen were superimposed by an offset of the detected global end reaction stress. This certainly revealed a higher magnitude of transverse tensile residual stresses in the weld seam area. Furthermore, the influence of the interpass temperature on transverse residual stresses is notably higher at low heat input in restraint welds. Nevertheless, in this case, comparatively low restraint intensities were attendant.

In future experiments, using increased specimen dimensions and restraint intensities, the complex interaction between heat control and welding reaction stresses should be further analysed. Those results could help in deriving improved heat control concepts and recommendations for existing technical guidelines dealing with the safety and processing of high-strength structural steel welding.

Acknowledgments The studies were funded by the AIF-project IGF-No. 17267 N/FOSTA P922. Sincere thanks are given for this support and to the representing companies actively involved in the project board.

References

1. Horikawa K, Watanabe N (2009) Application of extra-high tensile strength steel for hydropower plants in Japan. In: Conference on high strength steels for hydropower plants—Takasaki, Japan, pp. 1–8
2. Klein M, Spindler H, Luger A, Rauch R, Stiaszny P, Eigelsberger M (2005) Thermomechanically hot rolled high and ultra high strength steel grades—processing, properties and application. Mater Sci Forum 500–501:543–550, <http://www.scientific.net/MSF.500-501.543>
3. Hulka K, Kern A, Schriever U (2005) Application of niobium in quenched and tempered high-strength steels. Mater Sci Forum 500–501:519–526, <http://www.scientific.net/MSF.500-501.519>
4. Hanus F, Schroeter F, Schuetz W (2005) State of art in the production and use of high-strength heavy plates for hydro-power applications. In: High strength steel for hydropower plants, pp. 1–13, Graz
5. Grong O (1997) Metallurgical modelling of welding. Institute of Materials ISBN: 9781861250360
6. EN 1011-2: Welding—recommendation for welding of metallic materials—part 2: arc welding of ferritic steels. 2001
7. Wongpanya P, Boellinghaus T, Lothongkum G (2008) Ways to reduce the cold cracking risk in high strength structural steel welds. International Conference of the International Institute of Welding, Johannesburg, South Africa
8. Uwer D, Hohne H (1992) Determination of suitable minimum preheating temperatures for the cold-crack-free welding of steels. Weld Res Abroad 38(5):31–35, ISSN: 0043–2318
9. Masubuchi K (1980) Analysis of welded structures: residual stresses, distortion, and their consequences. Pergamon Press, New York. ISBN 9780080261294
10. Schwenk C, Kannengiesser T, Rethmeier M (2009) Restraint conditions and welding residual stresses in self-restrained cold cracking tests. In: Materials research, pp. 766–773
11. Rhode M, Kromm A, Kannengiesser T (2013) Residual stresses in multi-layer component welds. In: Trends in welding research: proceedings of the 9th international conference, June 4–8, 2012 Chicago, Illinois, USA, pp. 48–54, ASM International, ISBN: 1-62708-998-8
12. Boellinghaus T, Kannengiesser T, Neuhaus M (2005) Effects of the structural restraint intensity on the stress strain build up in butt joints. Math Modell Weld Phenom 7:651–669, 3-901351-99-X
13. Wongpanya P, Boellinghaus T, Lothongkum G (2008) Heat treatment procedures for hydrogen assisted cold cracking avoidance in s 1100 ql steel root welds. In: Materials research, no. d
14. Kannengiesser T, Lausch T, Kromm A (2011) Effects of heat control on the stress build-up during high-strength steel welding under defined restraint conditions. In: Welding in the world, vol. 55, no. 07, pp. 58–65, Springer, ISSN: 0043-2288
15. Eurocode 3 (2010): Design of steel structures (EN 1993)
16. EN 10025-6: Hot rolled products of structural steels—part 6: technical delivery conditions for flat products of high yield strength structural steels in the quenched and tempered condition. 2009
17. ISO 16834: Welding consumables—wire electrodes, wires, rods and deposits for gas shielded arc welding of high strength steels—classification. 2012
18. ISO 15614-1 (2012) Specification and qualification of welding procedures for metallic materials—welding procedure test—part 1: arc and gas welding of steels and arc welding of nickel and nickel alloys
19. Satoh K, Ueda Y, Matsui S, Natsume M, Terasaki T, Fukuda K, Tsuji M (1977) Japanese studies on structural restraint severity in relation

- to weld cracking. In: *Welding in the world*, vol. 15, no. 7, pp. 155–189, Springer, ISSN: 0043-2288
20. Nitschke-Pagel T, Wohlfahrt H (2002) Residual stresses in welded joints—sources and consequences. *Mater Sci Forum* 404–407:215–226. doi:[10.4028/www.scientific.net/MSF.404-407.215](https://doi.org/10.4028/www.scientific.net/MSF.404-407.215)
 21. Nitschke-Pagel T, Wohlfahrt H (1991) The generation of residual stresses due to joining processes. In: *Residual stresses—measurement, calculation, evaluation*. V. Hauk, H. Hougardy, E. Macherauch (Ed.), pp. 121–133, DGM Informationsgesellschaft mbH, ISBN: 3-88355-169-4
 22. ISO 14175: *Welding consumables—gases and gas mixtures for fusion welding and allied processes*. 2008
 23. Lausch T, Kannengiesser T, Schmitz-Niederau M (2013) Multi-axial load analysis of thick-walled component welds made of 13CrMoV9-10. *J Mater Process Technol* 213:1234–1240. doi:[10.1016/j.jmatprotec.2013.01.008](https://doi.org/10.1016/j.jmatprotec.2013.01.008)